PAMM

RESEARCH ARTICLE OPEN ACCESS

A Chemo-Mechanically Fully Coupled Multiphase-Field Model for Multicomponent Systems Accounting for Balance Equations on Singular Surfaces

Thea Kannenberg[1,2] | Andreas Prahs[3] | Britta Nestler[1,2,3] | Daniel Schneider[1,2]

[1]Institute of Digital Materials Science (IDM), Karlsruhe University of Applied Sciences, Karlsruhe, Germany | [2]Institute for Applied Materials (IAM-MMS), Karlsruhe Institute of Technology (KIT), Karlsruhe, Germany | [3]Institute of Nanotechnology (INT-MSS), Karlsruhe Institute of Technology (KIT), Eggenstein-Leopoldshafen, Germany

Correspondence: Thea Kannenberg (thea.kannenberg@h-ka.de) | Daniel Schneider (daniel.schneider@kit.edu)

Received: 30 June 2025 | **Revised:** 1 December 2025 | **Accepted:** 27 January 2026

ABSTRACT

Chemo-mechanically coupled phenomena such as stress-driven diffusion and diffusion-induced stresses are of high interest, for example, in battery materials and metals. In this work, a chemo-mechanically fully coupled multiphase-field model for a multicomponent system is derived and validated with a sharp interface solution. Ensuring mechanical compatibility, the model accounts for balance equations on singular surfaces and the Hadamard jump conditions. The models' capability to address stress-driven diffusion and diffusion-induced stresses is demonstrated through the presentation of an illustrative diffusion example.

1 | Introduction

An important task in materials science is the prediction of material characteristics. In crystalline materials, it is well established that the microstructure controls the overall material properties. Insights into the evolution of crystalline microstructures and the underlying mechanisms can be gained by modeling and simulation. Many material systems exhibit microstructural changes due to chemical and mechanical driving forces. The employment of chemo-mechanical microstructure simulations facilitates the investigation of such evolutions. The (multi)phase-field method allows the numerically efficient modeling of systems with an evolving microstructure, cf., e.g., [1, 2]. The position of an interface, e.g., a grain boundary, is implicitly given by a field of order parameters. In that manner, no interface tracking is necessitated. The development and application of chemo-mechanical multiphase-field models represents an active research field, cf., e.g., [3–5]. Regarding the diffuse interface area, different assumptions are made: While the model by Wheeler, Boettinger, and McFadden (WBM) assumes equal chemical compositions in the interface regions, cf. [6], the Kim–Kim–Suzuki (KKS) approach [7] assumes equal diffusion potentials in the interface regions. Similarly, equal diffusion potentials are assumed in grand chemical potential models, cf. [8, 9], and in the work at hand. In a similar manner, a number of models have been formulated to address the handling of mechanical fields in the diffuse interface area: The Voigt–Taylor approximation assumes equal strains and the Reuss–Sachs approximation assumes equal stresses in the diffuse interface area, cf., e.g., [10]. In this work, a jump condition approach is employed, cf., e.g., [11–13], which is consistent with sharp interface modeling, cf., e.g., [14]. The coupling of mechanical and nonmechanical fields is a recent research topic regarding phase-field models, cf., e.g., [15, 16]. Different chemo-mechanical coupling approaches are compared in a recent work [17]. As described therein, a full coupling is characterized by a mutually dependent balance of linear momentum and diffusion equation, where stresses are concentration-dependent and the diffusion equation comprises mechanically driven fluxes. Both

mechanical and chemical driving forces govern the evolution of phases. Within this work, the recently presented fully coupled multiphase-field model for two components [17], which accounts for jump conditions in the diffuse interface area, is extended to the multicomponent case. The model is validated with a sharp interface solution that is derived. Moreover, it is demonstrated that this chemo-mechanically fully coupled model allows for the representation of stress-driven diffusion and diffusion-induced stresses in the multicomponent case. The work at hand is organized as follows. The model formulation is extended to the multicomponent case in Section 2. In Section 3, the model is validated, and an illustrative example that highlights the model's ability to capture stress-driven diffusion and diffusion-induced stresses is presented. The work is concluded in Section 4.

2 | Model formulation

2.1 | Functional

Based on a functional of Ginzburg–Landau type [18]

$$\mathcal{F}[\boldsymbol{\phi},\bar{\boldsymbol{c}},\boldsymbol{u}] = \int_{\mathcal{V}} f_{\text{grad}}(\boldsymbol{\phi},\nabla\boldsymbol{\phi}) + f_{\text{pot}}(\boldsymbol{\phi}) + \bar{f}_{\text{chem}}(\boldsymbol{\phi},\bar{\boldsymbol{c}}) + \bar{f}_{\text{el}}(\boldsymbol{\phi},\bar{\boldsymbol{c}},\text{grad}(\boldsymbol{u}))\,\mathrm{d}v \tag{1}$$

a multicomponent, multiphase-field model is derived for the simulation of isothermal chemo-mechanical transformation processes. The order parameters are written as an N-tuple $\boldsymbol{\phi} = \{\phi_1,\dots,\phi_N\}$ and their gradients as $\nabla\boldsymbol{\phi} = \{\nabla\phi_1,\dots,\nabla\phi_N\}$. An order parameter adopts the value $\phi_\alpha = 1$ within its assigned region α and $\phi_\alpha = 0$ outside of it. Within the diffuse interface region at least two phases coexist. Their order parameters vary continuously between one and zero and are constrained by $\sum_{\alpha=1}^{N}\phi_\alpha = 1$. The gradient energy density f_{grad}, cf. [19], and the potential energy density f_{pot}, cf. [2], are given by

$$f_{\text{grad}}(\nabla\boldsymbol{\phi}) = -\epsilon\sum_{\beta=2}^{N}\sum_{\alpha=1}^{\beta-1}\gamma_{\alpha\beta}\nabla\phi_\alpha\cdot\nabla\phi_\beta\,,$$

$$f_{\text{pot}}(\boldsymbol{\phi}) = \frac{16}{\epsilon\pi^2}\sum_{\beta=2}^{N}\sum_{\alpha=1}^{\beta-1}\gamma_{\alpha\beta}\phi_\alpha\phi_\beta\,, \tag{2}$$

respectively. The interfacial energy density is given by $f_{\text{intf}} = f_{\text{grad}} + f_{\text{pot}}$. The width of the interface in equilibrium l_{eq} is related to the interface parameter ϵ via $l_{\text{eq}} = \epsilon\pi^2/4$ and the interfacial energy is denoted by $\gamma_{\alpha\beta}$. The potential energy is set to ∞, if $\boldsymbol{\phi}$ is not within the Gibbs simplex $\mathcal{G} = \{\boldsymbol{\phi} : \sum_{\alpha=1}^{N}\phi_\alpha = 1, \phi_\alpha \geq 0\}$, cf. [2]. The chemical and mechanical energy densities are given by interpolation of the phase-specific energy densities, i.e., $\bar{f}_{\text{chem}} = \sum_{\alpha=1}^{N}\phi_\alpha f^\alpha_{\text{chem}}$ and $\bar{f}_{\text{el}} = \sum_{\alpha=1}^{N}\phi_\alpha f^\alpha_{\text{el}}$. In contrast to the two-component model [17], where a single scalar concentration variable is considered, this work considers a tuple of $K-1$ independent concentration variables, written as $\bar{\boldsymbol{c}} = \{\bar{c}_1,\dots,\bar{c}_{K-1}\}$. The last component is calculated as $\bar{c}_K = 1 - \sum_{I=1}^{K-1}\bar{c}_I$. Each of the $K-1$ independent concentrations $\bar{c}_I$ is given by interpolation of the phase-specific concentrations c_I^α

$$\bar{c}_I = \sum_{\alpha=1}^{N}\phi_\alpha c_I^\alpha\,. \tag{3}$$

In this context, capital Latin letters are used to indicate that no Einstein summation convention is used with regard to the components. Employing a small strain framework, the displacement $\boldsymbol{u}$ is related to the infinitesimal strain tensor $\bar{\boldsymbol{\varepsilon}}$ via

$$\bar{\boldsymbol{\varepsilon}} = \sum_{\alpha=1}^{N}\phi_\alpha\boldsymbol{\varepsilon}^\alpha = \text{sym}(\text{grad}(\boldsymbol{u}))\,. \tag{4}$$

Herein, phase-specific strains are denoted by $\boldsymbol{\varepsilon}^\alpha$ and $\text{sym}(\cdot) = ((\cdot)+(\cdot)^{\mathsf{T}})/2$ denotes the symmetric part of a tensor.

2.2 | Evolution Equation of Order Parameters

With the variational derivative $\delta(\cdot)/\delta\phi_\alpha = \partial(\cdot)/\partial\phi_\alpha - \text{div}\,(\partial(\cdot)/\partial(\nabla\phi_\alpha))$, cf., e.g., [20, Eq. (13.63)], the evolution equation of order parameters is modeled as the superposition of pairwise interactions of $\tilde{N}$ locally present phases, cf. [21]. The evolution equation reads

$$\frac{\partial\phi_\alpha}{\partial t} = -\frac{1}{\epsilon}\sum_{\beta=1,\beta\neq\alpha}^{\tilde{N}} M_{\alpha\beta}\left(\frac{1}{\tilde{N}}\left(\frac{\delta f_{\text{intf}}}{\delta\phi_\alpha} - \frac{\delta f_{\text{intf}}}{\delta\phi_\beta}\right) + \frac{4(\phi_\alpha+\phi_\beta)}{\pi}\sqrt{\phi_\alpha\phi_\beta}\,\Delta^{\alpha\beta}_{\text{bulk}}\right)\,. \tag{5}$$

A detailed discussion on the bulk driving force prefactors can be found in [22]. Ignoring the derivative of $\bar{f}_{\text{el}}$ with respect to $\nabla\phi_\alpha$, cf. [13], the driving force is given by $\Delta^{\alpha\beta}_{\text{bulk}} = \left(\partial/\partial\phi_\alpha - \partial/\partial\phi_\beta\right)(\bar{f}_{\text{chem}} + \bar{f}_{\text{el}})$. The derivative of the chemical and mechanical energy densities with respect to ϕ_α yields

$$\frac{\partial(\bar{f}_{\text{chem}}+\bar{f}_{\text{el}})}{\partial\phi_\alpha} = f^\alpha_{\text{chem}} + f^\alpha_{\text{el}} + \sum_{\gamma=1}^{N}\sum_{I=1}^{K}\phi_\gamma\frac{\partial(f^\gamma_{\text{chem}}+f^\gamma_{\text{el}})}{\partial c_I^\gamma}\frac{\partial c_I^\gamma}{\partial\phi_\alpha} + \sum_{\gamma=1}^{N}\phi_\gamma\frac{\partial f^\gamma_{\text{el}}}{\partial\boldsymbol{\varepsilon}^\gamma}\cdot\frac{\partial\boldsymbol{\varepsilon}^\gamma}{\partial\phi_\alpha}\,. \tag{6}$$

A chemo-mechanical potential difference is defined as the diffusion potential $\mu_I = \hat{\mu}_I - \hat{\mu}_K$. Furthermore, equal diffusion potentials are assumed, i.e., $\mu_I = \mu_I^\alpha = \mu^\alpha_{\text{chem},I} + \mu^\alpha_{\text{el},I}\ \forall\alpha$. Herein, the chemical diffusion potentials read $\mu^\alpha_{\text{chem},I} = \partial f^\alpha_{\text{chem}}/\partial c_I^\alpha$ and the mechanical diffusion potentials read $\mu^\alpha_{\text{el},I} = \partial f^\alpha_{\text{el}}/\partial c_I^\alpha$. Furthermore, the concentrations c_I^α are not independent but fulfill the constraint $\sum_{I=1}^{K}c_I^\alpha = 1$, cf. [23]. It follows for the sum of the derivatives $\sum_{I=1}^{K}\partial c_I^\alpha/\partial\phi_\alpha = 0$. Moreover, given the independence of $\boldsymbol{\phi}$ and $\bar{\boldsymbol{c}}$, and with Equation (3), it is concluded that $\sum_{\gamma=1}^{N}\phi_\gamma\partial c_I^\gamma/\partial\phi_\alpha = -c_I^\alpha$. Accounting for these relations, Equation (6) simplifies to

$$\frac{\partial(\bar{f}_{\text{chem}}+\bar{f}_{\text{el}})}{\partial\phi_\alpha} = f^\alpha_{\text{chem}} + f^\alpha_{\text{el}} - \sum_{I=1}^{K-1}\mu_I c_I^\alpha + \sum_{\gamma=1}^{N}\phi_\gamma\frac{\partial f^\gamma_{\text{el}}}{\partial\boldsymbol{\varepsilon}^\gamma}\cdot\frac{\partial\boldsymbol{\varepsilon}^\gamma}{\partial\phi_\alpha}\,. \tag{7}$$

The mechanical energy densities f^α_{el} are given by $f^\alpha_{\text{el}} = \frac{1}{2}(\boldsymbol{\varepsilon}^\alpha - \tilde{\boldsymbol{\varepsilon}}^\alpha_{\text{c}})\cdot(\mathbb{C}^\alpha[\boldsymbol{\varepsilon}^\alpha - \tilde{\boldsymbol{\varepsilon}}^\alpha_{\text{c}}])$. Herein, the phase-specific stiffness tensors are denoted by $\mathbb{C}^\alpha$ and concentration-dependent eigenstrains

$$\tilde{\boldsymbol{\varepsilon}}^\alpha_{\text{c}} = \sum_{I=1}^{K-1}(c_I^\alpha - c^\alpha_{\text{ref},I})\tilde{\boldsymbol{\varepsilon}}^\alpha_{\text{ref},I} \tag{8}$$

are considered. In this context, $\tilde{\boldsymbol{\varepsilon}}^{\alpha}_{\mathrm{ref},I}$ and $c^{\alpha}_{\mathrm{ref},I}$ denote the so-called reference strain tensor and the reference concentration, respectively. It is highlighted that in the multicomponent model, eigenstrains pertaining to multiple independent components are taken into account. Additional inelastic phenomena such as plasticity are not considered in this work. For the incorporation of crystal plasticity the reader is referred to [24–26]. The Cauchy stress tensor $\boldsymbol{\sigma}^{\alpha}$ is related to f^{α}_{el} via Hooke's law $\partial f^{\alpha}_{\mathrm{el}}/\partial \boldsymbol{\varepsilon}^{\alpha} = \mathbb{C}^{\alpha}[\boldsymbol{\varepsilon}^{\alpha} - \tilde{\boldsymbol{\varepsilon}}^{\alpha}_{\mathrm{c}}] = \boldsymbol{\sigma}^{\alpha}$. Furthermore, interpolation of the phase-specific stresses yields $\bar{\boldsymbol{\sigma}} = \sum_{\alpha=1}^{N} \phi_{\alpha}\boldsymbol{\sigma}^{\alpha}$. The quasi-static balance of linear momentum without body forces $\mathrm{div}\,(\bar{\boldsymbol{\sigma}}) = \mathbf{0}$ is solved for in the bulk and the balance of angular momentum $\bar{\boldsymbol{\sigma}} = \bar{\boldsymbol{\sigma}}^{\mathrm{T}}$ is considered. This work employs the jump condition approach [13]. The phase-specific strains can be expressed as $\boldsymbol{\varepsilon}^{\alpha} = \bar{\boldsymbol{\varepsilon}} + \sum_{\gamma=1,\gamma\neq\alpha}^{N} \phi_{\gamma}\{\boldsymbol{\varepsilon}\}^{\alpha\gamma}$. In the diffuse interface context, the jump of a quantity ψ of arbitrary tensorial order across an interface is defined as $\{\psi\}^{\alpha\beta} = \psi^{\alpha} - \psi^{\beta}$. The jump of the strain tensor $\{\boldsymbol{\varepsilon}\}^{\alpha\beta}$ and the normal vector $\mathbf{n}^{\alpha\beta}$ between phases α and β are given by

$$\{\boldsymbol{\varepsilon}\}^{\alpha\beta} = \mathrm{sym}(\boldsymbol{a}^{\alpha\beta} \otimes \boldsymbol{n}^{\alpha\beta}), \quad \boldsymbol{n}^{\alpha\beta} = \frac{\nabla\phi_{\alpha} - \nabla\phi_{\beta}}{\|\nabla\phi_{\alpha} - \nabla\phi_{\beta}\|}. \tag{9}$$

The jump vector is denoted by $\boldsymbol{a}^{\alpha\beta}$. Consequently, Equation (7) can be further simplified to

$$\begin{aligned}\frac{\partial(\bar{f}_{\mathrm{chem}} + \bar{f}_{\mathrm{el}})}{\partial\phi_{\alpha}} &= f^{\alpha}_{\mathrm{chem}} + f^{\alpha}_{\mathrm{el}} - \sum_{I=1}^{K-1} \mu_I c^{\alpha}_I \\ &\quad + \sum_{\gamma=1,\gamma\neq\alpha}^{N} \phi_{\gamma}\boldsymbol{\sigma}^{\gamma} \cdot \{\boldsymbol{\varepsilon}\}^{\gamma\alpha}.\end{aligned} \tag{10}$$

In conclusion, the bulk driving force employed in Equation (5) reads

$$\begin{aligned}\Delta^{\alpha\beta}_{\mathrm{bulk}} &= \{f_{\mathrm{chem}}\}^{\alpha\beta} + \{f_{\mathrm{el}}\}^{\alpha\beta} \\ &\quad - \sum_{I=1}^{K-1} \mu_I \{c_I\}^{\alpha\beta} - \bar{\boldsymbol{\sigma}} \cdot \{\boldsymbol{\varepsilon}\}^{\alpha\beta}.\end{aligned} \tag{11}$$

The multicomponent model is distinguished by its ability to account for multiple chemo-mechanical potentials when analyzing the evolution of order parameters. For a more detailed derivation the reader is referred to the analogous two-component model in [17], where a single chemo-mechanical potential is considered.

2.3 | Evolution Equation of Concentration

The diffusion is modeled based on Fick's law as $\partial\bar{c}_I/\partial t = -\mathrm{div}\left(-\sum_{J=1}^{K-1}\bar{M}_{IJ}\nabla\mu_J\right)$. Herein, the chemical mobility is given by $\bar{M}_{IJ} = \sum_{\alpha=1}^{N}\phi_{\alpha}M^{\alpha}_{IJ}$. The phase-specific mobilities M^{α}_{IJ} can be determined by $D^{\alpha}_{IJ} = \sum_{L=1}^{K-1} M^{\alpha}_{IL}\partial\mu_L/\partial c^{\alpha}_J$, cf., e.g., [27]. For simplicity, the interdiffusivities are neglected, and thus, $M^{\alpha}_{IJ} = 0$ for $I \neq J$. In conclusion, the evolution equation reads

$$\frac{\partial c_I}{\partial t} = \mathrm{div}\left(\sum_{\alpha=1}^{N}\phi_{\alpha}D^{\alpha}_{II}\left(\frac{\partial\mu_I}{\partial c^{\alpha}_I}\right)^{-1}\nabla\mu_I\right). \tag{12}$$

TABLE 1 | Material and simulation parameters.

Parameter	Symbol	Unit	Value
Young's modulus	E	GPa	146.0
Poisson's ratio	ν	—	0.33
Diffusivity	D	$\mathrm{m^2 s^{-1}}$	1.0×10^{-11}
Molar volume	V_{m}	$\mathrm{m^3 mol^{-1}}$	7.0×10^{-6}
Interfacial energy	$\gamma_{\alpha\beta}$	$\mathrm{J\,m^{-2}}$	0.49
Domain size	L	nm	400
Spacial discretization	Δx	nm	2

In this work, substitutional and interstitial diffusion are not distinguished. It is emphasized, that the diffusion is governed by the gradient of a chemo-mechanical diffusion potential.

2.4 | Local Problem

Locally, the sum constraint for c^{α}_I ($K-1$ equations), the balance of linear momentum on a material singular surface ($\tilde{N}-1$ equations), and the equilibrium condition for the diffusion potentials ($(K-1)\tilde{N}$ equations) are solved. In summary, the local problem comprises the following equations

$$r_{c_I} := \sum_{\alpha=1}^{N}\phi_{\alpha}c^{\alpha}_I - \bar{c}_I = 0 \quad \forall I \in [1, K-1] \tag{13}$$

$$\boldsymbol{r}^{\mathrm{R}\alpha}_{\boldsymbol{\sigma}} := \{\boldsymbol{\sigma}\}^{\mathrm{R}\alpha}\boldsymbol{n}^{\mathrm{R}\alpha} = \mathbf{0} \quad \forall\alpha \in [1,\tilde{N}], \alpha \neq \mathrm{R} \tag{14}$$

$$r^{\alpha}_{\mu_I} := \mu^{\alpha}_{\mathrm{el},I} + \mu^{\alpha}_{\mathrm{chem},I} - \mu_I = 0 \quad \forall\alpha \in [1,\tilde{N}], I \in [1, K-1]. \tag{15}$$

The jump conditions are solved with respect to a reference phase R. Thus, the number of unknown jump vectors $\boldsymbol{a}^{\mathrm{R}\alpha}$ reduces to $\tilde{N}-1$. The local problem is solved for the unknowns $\{c^{\alpha}_I, \boldsymbol{a}^{\mathrm{R}\alpha}, \mu_I\}$.

3 | Results

3.1 | Assumptions

3.1.1 | Material

In the subsequent examples, an Fe–Mn–C alloy is considered. An austenitic phase is denoted with α and a ferritic with β. The material parameters are reported in Table 1. For simplicity, a constant diffusivity is assumed, i.e., $D^{\alpha}_{II} = D\ \forall\alpha, I$. Moreover, equal elastic constants are assumed. The mobility $M_{\alpha\beta}$ is treated as a numerical parameter and selected ensuring numerical stability.

3.1.2 | Fitting of Chemical Free Energy Densities

The chemical free energy densities $f^{\alpha}_{\mathrm{chem}}$ are approximated by parabolic functions

$$f^{\alpha}_{\mathrm{chem}} = \frac{1}{V_{\mathrm{m}}}\left(A^{\alpha}(c^{\alpha}_{\mathrm{C}})^2 + B^{\alpha}(c^{\alpha}_{\mathrm{Mn}})^2 + C^{\alpha}c^{\alpha}_{\mathrm{C}}c^{\alpha}_{\mathrm{Mn}} + D^{\alpha}c^{\alpha}_{\mathrm{C}} + E^{\alpha}c^{\alpha}_{\mathrm{Mn}} + F^{\alpha}\right) \tag{16}$$

TABLE 2 | Fitting parameters used for the parabolic fitting of chemical free energy densities, cf. Equation (16), at $T = 898\,\mathrm{K}$ with the Thermo-Calc [28] TCFE7 CALPHAD database.

Parameter	Unit	Austenite – α	Ferrite – β
$c_{\mathrm{C}}^{\mathrm{TC}}$	at.-%	4.23	3.71×10^{-2}
$c_{\mathrm{Mn}}^{\mathrm{TC}}$	at.-%	7.37	1.33
A	$\mathrm{J\,mol^{-1}}$	220500.00	28046875.00
B	$\mathrm{J\,mol^{-1}}$	52750.00	196625.00
C	$\mathrm{J\,mol^{-1}}$	−36250.00	56250.00
D	$\mathrm{J\,mol^{-1}}$	16865.12	16231.11
E	$\mathrm{J\,mol^{-1}}$	−34964.16	−33723.89
F	$\mathrm{J\,mol^{-1}}$	−35336.05	−35790.99

in the vicinity of the equilibrium concentrations, cf., e.g., [29]. Herein, equal molar volumes are considered, i.e., $V_{\mathrm{m}} = V_{\mathrm{m}}^{\alpha}\ \forall\alpha$. A least square method is employed to fit the coefficients to a CALPHAD database at the absolute temperature $T = 898\,\mathrm{K}$. The resulting parameters, fitted with the TCFE7 database in Thermo-Calc [28], and the equilibrium concentrations c_I^{TC} are summarized in Table 2.

3.1.3 | Diffusion Potentials

In the following examples, a constant stiffness tensor and concentration-dependent eigenstrains, cf. Equation (8), are considered. Thus, the mechanical diffusion potentials read

$$\mu_{\mathrm{el},I}^{\alpha} = \frac{\partial f_{\mathrm{el}}^{\alpha}}{\partial c_I^{\alpha}} = -\tilde{\boldsymbol{\varepsilon}}_{\mathrm{ref},I}^{\alpha} \cdot \boldsymbol{\sigma}^{\alpha}\,, \quad I \in [\mathrm{C}, \mathrm{Mn}]\,. \tag{17}$$

With Equation (16), the chemical diffusion potentials read

$$\mu_{\mathrm{chem,C}}^{\alpha} = \frac{2A^{\alpha}c_{\mathrm{C}}^{\alpha} + C^{\alpha}c_{\mathrm{Mn}}^{\alpha} + D^{\alpha}}{V_{\mathrm{m}}}\,, \quad \mu_{\mathrm{chem,Mn}}^{\alpha} = \frac{2B^{\alpha}c_{\mathrm{Mn}}^{\alpha} + C^{\alpha}c_{\mathrm{C}}^{\alpha} + E^{\alpha}}{V_{\mathrm{m}}}\,. \tag{18}$$

3.2 | Validation

3.2.1 | Setup

For validation of the model, the approach presented in [17, 30] is adapted to account for the two independent components C and Mn in a two phase system with phases α and β. In this regard, the sharp interface solution of a 2D inclusion problem is compared to a phase-field simulation, which is run until equilibrium is reached. The equilibrium conditions for a two-phase, multicomponent system are derived from the generalized Gibbs–Thomson equation, cf., e.g., [31, 32], and read

$$\begin{aligned} g_1 := {} & \{f_{\mathrm{chem}}\}^{\alpha\beta} - (\mu_{\mathrm{chem,C}}^{\alpha} + \mu_{\mathrm{el,C}}^{\alpha})\{c_{\mathrm{C}}\}^{\alpha\beta} \\ & - (\mu_{\mathrm{chem,Mn}}^{\alpha} + \mu_{\mathrm{el,Mn}}^{\alpha})\{c_{\mathrm{Mn}}\}^{\alpha\beta} \\ & + \{f_{\mathrm{el}}\}^{\alpha\beta} - \bar{\boldsymbol{\sigma}} \cdot \{\boldsymbol{\varepsilon}\}^{\alpha\beta} + 2\gamma_{\alpha\beta}\bar{\kappa}_S = 0 \end{aligned} \tag{19}$$

$$g_2 := \mu_{\mathrm{chem,C}}^{\alpha} + \mu_{\mathrm{el,C}}^{\alpha} - \mu_{\mathrm{chem,C}}^{\beta} - \mu_{\mathrm{el,C}}^{\beta} = 0 \tag{20}$$

$$g_3 := \mu_{\mathrm{chem,Mn}}^{\alpha} + \mu_{\mathrm{el,Mn}}^{\alpha} - \mu_{\mathrm{chem,Mn}}^{\beta} - \mu_{\mathrm{el,Mn}}^{\beta} = 0 \tag{21}$$

$$g_4 := c_{\mathrm{tot,C}} - \xi^{\alpha}c_{\mathrm{C}}^{\alpha} - \xi^{\beta}c_{\mathrm{C}}^{\beta} = 0\,. \tag{22}$$

In the sharp interface context, $\bar{\boldsymbol{\sigma}} = (\boldsymbol{\sigma}^{\alpha} + \boldsymbol{\sigma}^{\beta})/2$, cf., e.g., [14], is used and the mechanical solutions of the boundary value problem, as given, e.g., in [17, 33, 34], are substituted. The curvature $\bar{\kappa}_S$ of the circular inclusion is expressed in terms of the radius a and is given by

$$\bar{\kappa}_S = \frac{1}{2}a^{-1} = \frac{1}{2}\left(\xi^{\alpha}\frac{A_{\mathrm{tot}}}{\pi}\right)^{-\frac{1}{2}}\,, \tag{23}$$

cf., e.g., [30, Eqs. (41)–(42)]. Herein, A_{tot} refers to the total area of the simulation domain and is given by $A_{\mathrm{tot}} = L^2$, cf. Figure 1a. The phase-fraction ξ^{α} depends on the phase-specific concentrations via the lever rule

$$\xi^{\alpha} = \frac{\sqrt{(c_{\mathrm{Mn}}^{\beta} - c_{\mathrm{tot,Mn}})^2 + (c_{\mathrm{C}}^{\beta} - c_{\mathrm{tot,C}})^2}}{\sqrt{(c_{\mathrm{Mn}}^{\beta} - c_{\mathrm{Mn}}^{\alpha})^2 + (c_{\mathrm{C}}^{\beta} - c_{\mathrm{C}}^{\alpha})^2}}\,. \tag{24}$$

The equilibrium conditions above are solved for the equilibrium concentrations $\{c_{\mathrm{C}}^{\alpha}, c_{\mathrm{Mn}}^{\alpha}, c_{\mathrm{C}}^{\beta}, c_{\mathrm{Mn}}^{\beta}\}$. For the phase-field simulation, the simulation domain, cf. Figure 1a, is initialized with homogeneous concentration fields $\bar{c}_{\mathrm{C}} = 1.2$ at.-% and $\bar{c}_{\mathrm{Mn}} = 3.0$ at.-%, which correspond to the average concentrations $c_{\mathrm{tot,C}}$ and $c_{\mathrm{tot,Mn}}$, respectively. Zero-flux boundary conditions are enforced for the component fluxes. Dirichlet boundary conditions are applied according to the analytical solutions given, e.g., in [33, 34]. The circular inclusion is austenitic and subjected to concentration-dependent eigenstrains, cf. Equation (8), with $\tilde{\boldsymbol{\varepsilon}}_{\mathrm{ref,C}}^{\alpha} = 0.2\boldsymbol{I}$ and $\tilde{\boldsymbol{\varepsilon}}_{\mathrm{ref,Mn}}^{\alpha} = -0.05\boldsymbol{I}$ and $c_{\mathrm{ref,C}}^{\alpha} = c_{\mathrm{ref,C}}^{\alpha} = 0$. These values are not representative for the material system and are chosen for illustrative purposes. The matrix is ferritic and $\tilde{\boldsymbol{\varepsilon}}_{\mathrm{c}}^{\beta} = \mathbf{0}$ is considered.

3.2.2 | Results

The results of the validation are reported in Figure 1. The inclusion grows until it reaches its equilibrium size. In Figure 1b, the inclusion is illustrated at time $t = t_0$ and in equilibrium at time $t = t_{\mathrm{eq}}$. The sharp interface consideration, i.e., the solution to Equations (19)–(22), predicts a phase fraction in equilibrium $\xi_{\mathrm{eq,SI}}^{\alpha} = 30.40\,\%$, while the phase-field simulation predicts $\xi_{\mathrm{eq,PFS}}^{\alpha} = \int_{\mathcal{V}} \phi_{\alpha}\,\mathrm{d}v / (\int_{\mathcal{V}} \mathrm{d}v) = 30.23\,\%$. Consequently, the relative error is less then 1 %. The concentration profiles along a horizontal line with $y = 200\,\mathrm{nm}$ obtained with the phase-field simulation are compared to the equilibrium concentrations predicted by the sharp interface consideration in cf. Figure 1c. In equilibrium, a convincing agreement of the equilibrium concentrations with the sharp interface solution is observed.

3.3 | Diffusion Example

3.3.1 | Setup

In the following example, the chemo-mechanically fully coupled model's ability to capture stress-driven diffusion and diffusion-

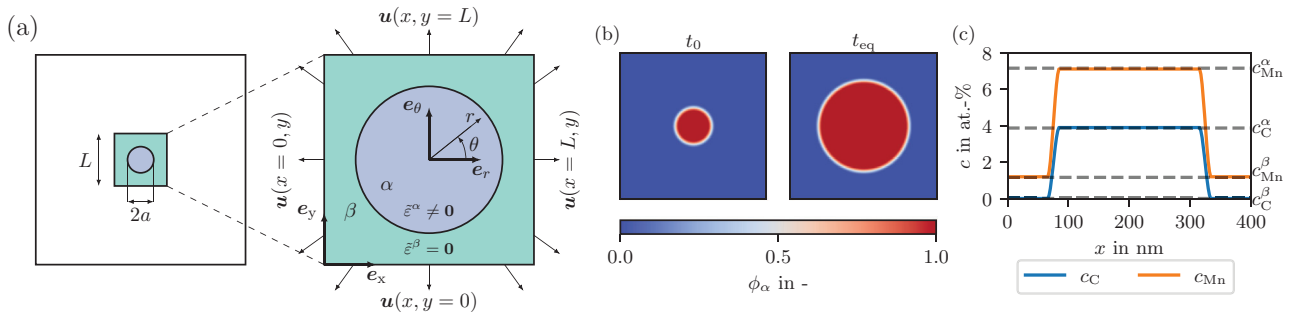

FIGURE 1 | For validation, an inclusion problem is considered, cf. [17]. A finite section of length L with Dirichlet boundary conditions is used as simulation domain (a). The inclusion grows until it reaches its equilibrium size (b). The concentration profiles at $y = 200\,\text{nm}$ in equilibrium are visualized (c). Moreover, the corresponding sharp interface solutions are given by dashed lines.

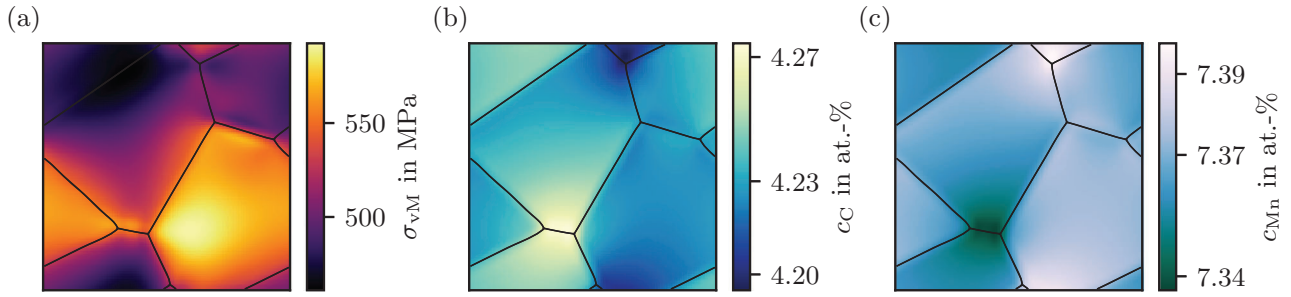

FIGURE 2 | The impact of mechanical fields on component diffusion is examined. Initially, the concentration fields are homogeneous. The resulting von Mises stress σ_{vM} in equilibrium is heterogenous and visualized in (a). The C distribution (b) and Mn distribution (c) are inhomogeneous in equilibrium. Regions of elevated C content exhibit reduced Mn content.

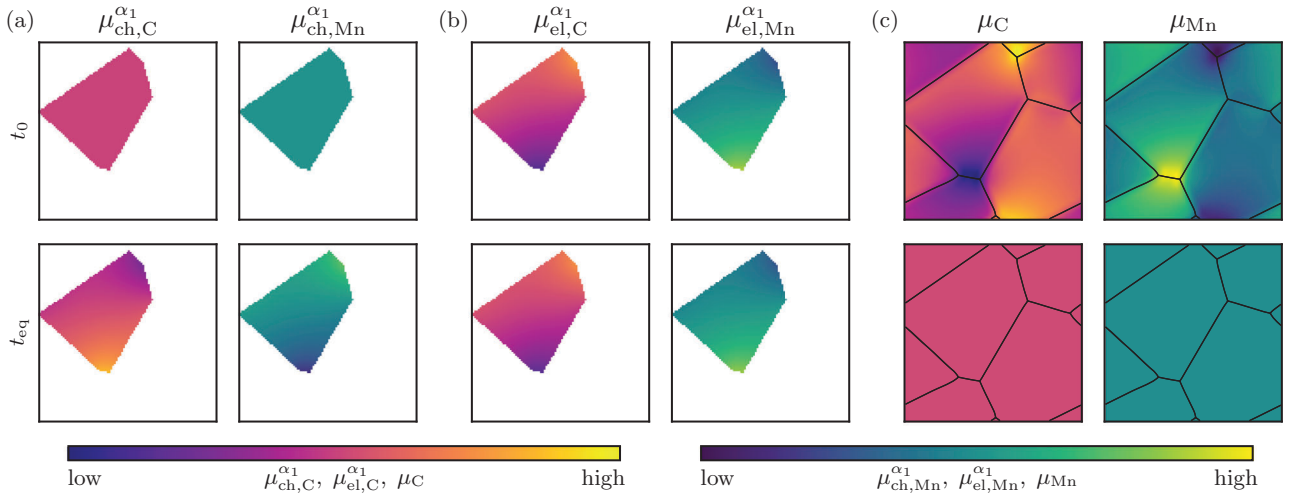

FIGURE 3 | Diffusion potentials are visualized at time $t = t_0$ (top row) and in equilibrium $t = t_{eq}$ (bottom row). The chemical diffusion potentials $\mu^{\alpha_1}_{ch,C}$ and $\mu^{\alpha_1}_{ch,Mn}$ of each phase are homogeneous at $t = t_0$ and inhomogeneous at $t = t_{eq}$ (a). The mechanical diffusion potentials $\mu^{\alpha_1}_{el,C}$ and $\mu^{\alpha_1}_{el,Mn}$ have gradients (b). The chemical and mechanical diffusion potentials in (a) and (b) are phase-specific and visualized for a single phase α_1 in the bulk. As a result, the chemo-mechanical diffusion potentials are inhomogeneous at $t = t_0$ and homogeneous in equilibrium $t = t_{eq}$ (c).

induced stresses is highlighted. In this regard, a polycrystal with austenitic grains is considered without phase transformation. Each grain is subjected to a concentration-dependent eigenstrain. The reference strain tensor, cf. Equation (8) is assumed to be anisotropic. Moreover, each grain is randomly rotated around the out-of-plane axis. For illustrative purposes, opposite signs of the reference strain tensors for C and Mn are assumed. The reference concentrations are set to zero. The setup is analogous to the two-component diffusion example in [17]. The domain is initialized with homogeneous concentration fields $\bar{c}_C = c_C^{TC,\alpha}$ and $\bar{c}_{Mn} = c_{Mn}^{TC,\alpha}$, cf. Table 2. A periodic boundary condition is considered for all concentration fluxes. Furthermore, the domain is subjected to a periodic boundary condition that fulfills a macroscopic strain $\bar{\boldsymbol{\varepsilon}} = 0.005\boldsymbol{e}_x \otimes \boldsymbol{e}_x$.

3.3.2 | Results

The results of this diffusion example are visualized in Figures 2 and 3. The initially homogeneous concentration fields cause an inhomogeneous stress distribution, as visualized in terms of the von Mises stress σ_{vM} in Figure 2a. Due to the inhomogeneous stress fields, component fluxes of C and Mn are inhomogeneous. This results in an heterogeneous concentration distribution of C, cf. Figure 2b, and Mn, cf. Figure 2c, in equilibrium. The reference strains for C and Mn have opposite signs for illustrative purpose. Consequently, the gradients of the chemo-mechanical diffusion potentials, and thus, the component fluxes, have opposite signs, cf. Figure 3. As a result, regions with elevated carbon concentrations c_{C} exhibit reduced levels of manganese c_{Mn} in equilibrium. In this example, component fluxes are induced due to concentration-dependent stresses. Initially, the chemo-mechanical diffusion potentials μ_I are heterogeneous due to a gradient in the mechanical diffusion potentials. In equilibrium, the chemo-mechanical diffusion potentials are homogeneous, cf. Figure 3.

4 | Conclusion

The chemo-mechanically fully coupled multiphase-field model for two components, which is presented in a previous work [17], is extended to enable the modeling of multicomponent systems. The model accounts for balance equations on singular surfaces and the Hadamard jump conditions in the diffuse interface regions. The model is validated using a sharp interface solution. A convincing agreement with the sharp interface solution is observed. The model's functionality is further investigated with the help of a diffusion example. It is clearly visible how diffusion-induced stresses and stress-driven diffusion can be addressed with this chemo-mechanically fully coupled multiphase-field model for multicomponent systems.

Acknowledgments

Thea Kannenberg gratefully acknowledges funding by the German Research Foundation (DFG) within the project "Giga-NANOBAIN" (proj. no. 490856143). Andreas Prahs gratefully acknowledges the financial support by the Federal Ministry of Education and Research (BMBF) within the joint Project "05M2022 - DASEA-4-SOFC". Daniel Schneider and Britta Nestler are thankful for funding through the Helmholtz Association, within program "Materials Systems Engineering (MSE)" (proj. no. 43.31.01).

Open access funding enabled and organized by Projekt DEAL.

References

1. I. Steinbach, F. Pezzolla, B. Nestler, et al., "A Phase Field Concept for Multiphase Systems," *Physica D: Nonlinear Phenomena* 94, no. 3 (1996): 135–147.

2. B. Nestler, H. Garcke, and B. Stinner, "Multicomponent Alloy Solidification: Phase-Field Modeling and Simulations," *Physical Review E* 71, no. 4 (2005): 041609.

3. B. Svendsen, P. Shanthraj, and D. Raabe, "Finite-Deformation Phase-Field Chemomechanics for Multiphase, Multicomponent Solids," *Journal of the Mechanics and Physics of Solids* 112 (2018): 619–636.

4. B. Böttger, M. Apel, M. Budnitzki, J. Eiken, G. Laschet, and B. Zhou, "Calphad Coupled Phase-Field Model With Mechano-Chemical Contributions and Its Application to Rafting of γ' in CMSX-4," *Computational Materials Science* 184 (2020): 109909.

5. S. Chatterjee, D. Schwen, and N. Moelans, "An Efficient and Quantitative Phase-Field Model for Elastically Heterogeneous Two-Phase Solids Based on a Partial Rank-One Homogenization Scheme," *International Journal of Solids and Structures* 250 (2022): 111709.

6. A. A. Wheeler, W. J. Boettinger, and G. B. McFadden, "Phase-Field Model for Isothermal Phase Transitions in Binary Alloys," *Physical Review A* 45, no. 10 (1992): 7424–7439.

7. S. G. Kim, W. T. Kim, and T. Suzuki, "Phase-Field Model for Binary Alloys," *Physical Review E* 60, no. 6 (1999): 7186–7197.

8. M. Plapp, "Unified Derivation of Phase-Field Models for Alloy Solidification From a Grand-Potential Functional," *Physical Review E* 84, no. 3 (2011): 031601.

9. A. Choudhury and B. Nestler, "Grand-Potential Formulation for Multicomponent Phase Transformations Combined With Thin-Interface Asymptotics of the Double-Obstacle Potential," *Physical Review E* 85, no. 2 (2012): 021602.

10. K. Ammar, B. Appolaire, G. Cailletaud, and S. Forest, "Combining Phase Field Approach and Homogenization Methods for Modelling Phase Transformation in Elastoplastic Media," *European Journal of Computational Mechanics* 18, no. 5-6 (2009): 485–523.

11. J. Mosler, O. Shchyglo, and H. M. Hojjat, "A Novel Homogenization Method for Phase Field Approaches Based on Partial Rank-One Relaxation," *Journal of the Mechanics and Physics of Solids* 68 (2014): 251–266.

12. A. Durga, P. Wollants, and N. Moelans, "Evaluation of Interfacial Excess Contributions in Different Phase-Field Models for Elastically Inhomogeneous Systems," *Modelling and Simulation in Materials Science and Engineering* 21, no. 5 (2013): 055018.

13. D. Schneider, F. Schwab, E. Schoof, et al., "On the Stress Calculation Within Phase-Field Approaches: A Model for Finite Deformations," *Computational Mechanics* 60, no. 2 (2017): 203–217.

14. M. Silhavy, *The Mechanics and Thermodynamics of Continuous Media* (Springer, 1997).

15. A. Prahs, M. Reder, D. Schneider, and B. Nestler, "Thermomechanically Coupled Theory in the Context of the Multiphase-Field Method," *International Journal of Mechanical Sciences* 257 (2023): 108484.

16. A. Prahs, D. Schneider, and B. Nestler, "A Continuum Thermodynamic Approach to the Phase-Field Method: The Order Parameter as Internal State Variable," *Continuum Mechanics and Thermodynamics* 37, no. 4 (2025): 55.

17. T. Kannenberg, A. Prahs, B. Svendsen, B. Nestler, and D. Schneider, "Coupling Approaches in Chemo-Mechanical Multiphase-Field Models," *International Journal of Mechanical Sciences* 303 (2025): 110569.

18. V. L. Ginzburg, "On the Theory of Superconductivity," *Il Nuovo Cimento* 2, no. 6 (1955): 1234–1250.

19. I. Steinbach and F. Pezzolla, "A Generalized Field Method for Multiphase Transformations Using Interface Fields," *Physica D: Nonlinear Phenomena* 134, no. 4 (1999): 385–393.

20. H. Goldstein, C. P. Poole, and J. L. Safko, *Classical Mechanics (3rd Edition)* (Addison Wesley, 2002).

21. I. Steinbach, "Phase-Field Models in Materials Science," *Modelling and Simulation in Materials Science and Engineering* 17, no. 7 (2009): 073001.

22. P. W. Hoffrogge, S. Daubner, D. Schneider, B. Nestler, B. Zhou, and J. Eiken, "Triple Junction Benchmark for Multiphase-Field Models Combining Capillary and Bulk Driving Forces," *Modelling and Simulation in Materials Science and Engineering* 33, no. 1 (2025): 015001.

23. J. Eiken, B. Böttger, and I. Steinbach, "Multiphase-Field Approach for Multicomponent Alloys With Extrapolation Scheme for Numerical Application," *Physical Review E* 73, no. 6 (2006): 066122.

24. A. Prahs, L. Schöller, F. K. Schwab, D. Schneider, T. Böhlke, and B. Nestler, "A Multiphase-Field Approach to Small Strain Crystal Plasticity Accounting for Balance Equations on Singular Surfaces," *Computational Mechanics* 73 (2023): 773–794.

25. T. Kannenberg, L. Schöller, A. Prahs, D. Schneider, and B. Nestler, "Investigation of Microstructure Evolution Accounting for Crystal Plasticity in the Multiphase-Field Method," *PAMM* 23, no. 3 (2023): e202300138.

26. T. Kannenberg, L. Schöller, A. Prahs, D. Schneider, and B. Nestler, "Microstructure Evolution Accounting for Crystal Plasticity in the Context of the Multiphase-Field Method," *Computational Mechanics* 74, no. 1 (2024): 67–84.

27. L. K. Aagesen, Y. Gao, D. Schwen, and K. Ahmed, "Grand-Potential-Based Phase-Field Model for Multiple Phases, Grains, and Chemical Components," *Physical Review E* 98, no. 2 (2018): 023309.

28. J.-O. Andersson, T. Helander, L. Höglund, P. Shi, and B. Sundman, "Thermo-Calc & Dictra, Computational Tools for Materials Science," *Calphad* 26, no. 2 (2002): 273–312.

29. K. D. Noubary, M. Kellner, J. Hötzer, M. Seiz, H. J. Seifert, and B. Nestler, "Data Workflow to Incorporate Thermodynamic Energies From Calphad Databases Into Grand-Potential-Based Phase-Field Models," *Journal of Materials Science* 56, no. 20 (2021): 11 932–11 952.

30. T. Kannenberg, A. Prahs, B. Svendsen, B. Nestler, and D. Schneider, "Chemo-Mechanical Benchmark for Phase-Field Approaches," *Modelling and Simulation in Materials Science and Engineering* 33, no. 1 (2025): 015004.

31. W. C. Johnson and J. I. D. Alexander, "Interfacial Conditions for Thermomechanical Equilibrium in Two-Phase Crystals," *Journal of Applied Physics* 59, no. 8 (1986): 2735–2746.

32. P. W. Voorhees and W. C. Johnson, "Interfacial Equilibrium During a First-Order Phase Transformation in Solids," *Journal of Chemical Physics* 84, no. 9 (1986): 5108–5121.

33. S. Li, R. Sauer, and G. Wang, "A Circular Inclusion in a Finite Domain I. The Dirichlet-Eshelby Problem," *Acta Mechanica* 179, no. 1-2 (2005): 67–90.

34. F. D. Fischer, G. A. Zickler, and J. Svoboda, "Elastic Stress–Strain Analysis of an Infinite Cylindrical Inclusion With Eigenstrain," *Archive of Applied Mechanics* 88, no. 3 (2018): 453–460.